



Biochar from Digestate Pyrolysis as a Filler for Biopolymer Blends: Effect of Blend Composition

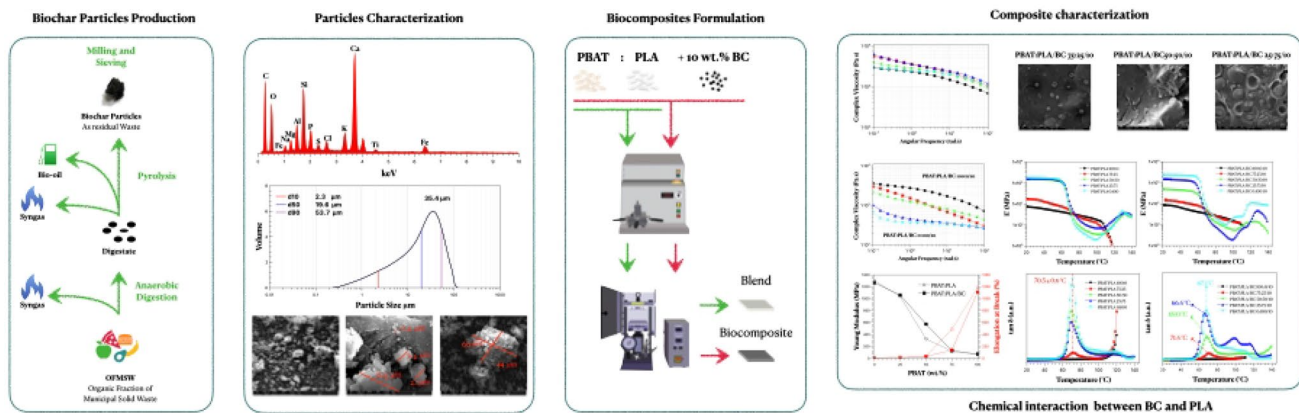
Giulia Infurna¹ · Luigi Botta¹ · Irene Ingargiola¹ · Marco Maniscalco¹ · Giuseppe Caputo¹ · Nadka Tz. Dintcheva¹

Accepted: 19 October 2023
© The Author(s) 2023

Abstract

This study investigates the effect of biochar (BC) as a filler for biopolymer blends, with a focus on the effect of the biopolymer weight ratio on the final BC-added blends. The blends studied in this work were obtained by varying the weight ratio of poly-butylene adipate-co-terephthalate (PBAT) and polylactic acid (PLA) due to their great importance in packaging and agricultural fields. BC has been produced in our laboratories by the slow pyrolysis of the digestate obtained from the anaerobic digestion of the organic fraction of municipal solid waste (OFMSW). After pyrolysis, digestate-derived biochar has been milled and sieved to produce a powdery form with diameter of less than 45 μm . In order to better investigate the filler/polymer interactions, biochar particles were dimensionally, morphologically and chemically characterised. The inhomogeneity of the feedstock is responsible for content and high diversity of inorganics in biochar surface. The effect of BC on PBAT and PLA biopolymer matrices is different, and for the blend compositions the relative weight ratio between PBAT and PLA plays an important role. Furthermore, the biocomposite blend has been fully characterised: rheological, morphological, mechanical and dynamic-mechanical characterisations have been carried out, highlighting how the properties results strongly influenced by the presence of BC in the blend. In addition, a study of the viscous molar mass of the two polymer matrices when processed in the presence or absence of BC particles highlighting that a strong chemical interaction occurs between PLA and BC particles, unlike PBAT and BC.

Graphical Abstract



Keywords Biochar · Biocomposites · PLA · PBAT · Polymer blends

Extended author information available on the last page of the article

Introduction

The circular economy with a set of proactive measures like the production of sustainable products, business models and standards have already been defined by the European Commission [1]. Therefore, a shift towards more sustainable materials and production processes needs to be made by the industries. The widespread use of polymers in the packaging industry and the huge impact that disposable products have on our daily lives, has led to increased efforts to replace conventional polymers with biodegradable polymers. This is in order to reduce the environmental pollution caused by the improper disposal of conventional polymers. With the same aim of reducing waste and its impact, pyrolysis of waste has increased interest as a way of valorising waste in the form of bio-oil and syngas. In addition, the use of biochar, the solid by-product of pyrolysis, as a value-added material is a fundamental part of the circular economy.

In recent years, biopolymers and blends of biopolymers, such as polysaccharides, proteins and lipids, have been widely investigated as materials not only for the green packaging industry [2–7], but also in the transportation, automotive or other more profitable fields, such as biomedical or cultural heritage preservation [8–13]. Of course, the use of biopolymers, even if they are biodegradable or compostable, does not exempt one from considering and proposing a disposal route. Whether biopolymers actually degrade spontaneously in natural habitats, especially when present in large quantities, compared to specific experimental conditions such as industrial composting, is an ongoing debate. For the polymer to be truly green, it must be recyclable [14]. In this perspective, polylactic acid, PLA, has attracted great interest due to its unique properties comparable to conventional plastics, combined with its renewability and compostability, and has found its way into medical applications (i.e. implant devices, tissue scaffolds, drug delivery) [15, 16], packaging and textile sectors [2, 17], automotive and electronics applications [10, 11]. However, the brittleness and low thermal stability of PLA combined with its high cost could limit its applications. To avoid this drawback, PLA can often be blended with other biopolymers or added with some filler to improve its properties and/or reduce the final cost of a product. Among several biopolymers used in blends with PLA, poly(butylene adipate-co-terephthalate), PBAT, is well used due to its high ductility and complete biodegradability [18, 19]. PBAT, biodegradable thermoplastic bio-polyester random copolymer obtained by polycondensation of butane diol (BDO), adipic acid (AA) and terephthalic acid (PTA), shows good biodegradability due to the presence of aliphatic functional groups and excellent

mechanical properties due to the aromatic structure in the molecular chain [4, 20, 21]. Several studies have been carried out on PLA blended with PBAT to improve the processability and tensile properties of PLA [22, 23].

A complete study of the morphological structure of these two biopolymers has been carried out by Pietrostanto et al. [24] to evaluate the suitability of PLA:PBAT blends as packaging materials for chilled and frozen foods, highlighting that the more PBAT is added to the blend, the lower the oxygen barrier is, even if an increase in the toughness of the final film has been found. Moustafa et al. [5] blended PLA and PBAT and improved the biocompatibility of the blend with expanded colophony organoclay, which was also responsible for a significant improvement in the viscoelastic and mechanical properties of the final nanocomposites. Xin Li et al. [25] prepared biodegradable films of PLA with PBAT in the presence of chain extenders to increase the ductility of the PLA film and improve the toughness and viscoelastic properties [26].

The biodegradation study of films based on PLA:PBAT blend has been carried out by several authors. The biodegradation of PBAT:PLA blends under soil conditions has been studied, revealing a different biodegradation mechanism of the two matrices, although a decrease in carbon content and a global increase in oxygen content have been found for pristine matrices and the blends [27]. The photo-oxidation behaviour of the polymer blend has also been studied by Xie [28], who proposes a predictive model to quickly evaluate the life of the blend films, since agricultural mulch films are one of the possible applications of this blend.

As mentioned above, in addition to the use of biodegradable polymer, another way to reduce waste and move towards more sustainable production is the valorisation of waste as a feedstock for energy production through pyrolysis. The Biochar (BC), a carbon-rich product, has increased its interest as a value-added material due to specific characteristics such as cation exchange capacity, large specific surface area, high porosity stable structure and high thermal stability [29, 30]. BC has been widely used in environmental applications such as soil remediation [31, 32], fuel cell additive [33–35], wastewater treatment [36, 37] and as a filler for biopolymer production [38, 39]. In addition, the structure and properties of biochar can be tailored to the application by varying the pyrolysis operating conditions, i.e. by varying the temperature, heating rate and oxygen flow, it's possible to control the global porosity of BC particles and the presence of residual functional groups on their surface [40–42]. Furthermore, when used as a filler in polymer matrix, BC can impart great electrical properties [43, 44], barrier properties [45], mechanical [46] and thermal properties [47, 48], and radical scavenging protection [40, 49].

A previous study investigated the properties and filmability of biocomposites based on PBAT as polymer matrix and

commercial biochar powder as filler, varying the filler content of BC in the composites and selecting the composites with 5 wt% and 10 wt% BC in PBAT matrix as the most suitable composites for film blowing production [49]. Furthermore, the use of three different biochar particles produced from carob waste, as a result of three different temperature pyrolysis, were incorporated into PBAT polymer matrix. This study has been determined the relationship between pyrolysis temperature condition [50] and biochar particles and the relative final composite properties [40]. In a study conducted by George et al. [51], a composite was prepared by blending PLA in a high concentration and PBAT, in the presence of BC particles. The study highlighted a reduction in the electrical resistivity of the matrix when 10 wt% of BC was added. Accordingly, Musiol et al. [52] Found that for PBAT:PLA/BC composites, the dependence of the surface resistivity of the composites strongly depends on the BC content, and found that the addition of 30 wt% of BC resulted in a sixfold reduction with respect to PBAT:PLA.

In this study, PBAT:PLA based biocomposites have been formulated by adding biochar particles, keeping the filler loading constant at 10 wt%, a concentration chosen based on the results of our previous work [40, 49]. A comprehensive study has been carried out on how the presence of biochar has a drastic effect on the properties of the blend as the PBAT:PLA weight ratio changes. The BC particles used in this work have been formulated in our laboratory as a result of the slow pyrolysis process performed on digestate, the results of decomposition under low oxygen atmosphere of a biodegradable waste to produce biogas. The operating conditions chosen for pyrolysis are therefore determined by optimizing energy for biogas production, and the resulting biochar fraction, i.e. a waste, was used to produce our composites. Initially, the biochar particles were dimensionally, chemically and morphologically characterized. Later, to characterise the biocomposite blends, rheological, morphological, thermal and mechanical characterisation were carried out, comparing the blend formulation with the filled blend formulation. Finally, to fully characterise the composites, the intrinsic viscous molar mass was evaluated using a capillary viscosimeter for PBAT and PLA, and for PBAT and PLA after processing with BC particles.

Materials and Methods

Materials

Poly(butylene adipate-co-terephthalate), PBAT, (commercial Ecoflex® F Blend C1200, BASF, SE, Ludwigshafen, Germany) is a film grade with a melt flow rate (MFR) of 2.7–4.9 g/10 min (190 °C, 2.16 kg), a density in the range 1.25–1.27 g/cm³ and a melting temperature in the range

110–120 °C. Poly(lactic acid), PLA, (commercial Ingeo® 4032D, NatureWorks, USA) with a melt flow index (MFI) of 7 g/10 min (at 210 °C and 2.16 kg), a density of 1.24 g/cm³ and a melting point between 155 and 170 °C. The biochar used in this work was produced in our laboratory, following the entire procedure.

Feedstock Thermo-gravimetric Analysis and Digestate Slow Pyrolysis

The feedstock for thermal cracking, digestate, was kindly provided by Archimede s.r.l., Caltanissetta, after extraction of biogas by anaerobic digestion of OFMSW, Organic Fraction of Municipal Solid Waste. The feedstock was characterised before the slow pyrolysis process. The thermogravimetric study of the waste was carried out using a Netzsch STA 449 F1 Jupiter thermogravimetric analyser. Approximately 90 ± 5 mg of the sample under consideration was crushed to reduce the waste to powder and transferred to the crucible of the analyser. Each thermogravimetric analysis was repeated at least in duplicate and the sample was heated at different heating rates (i.e. 5, 10, 20 and 40 °C/min) from room temperature to 600 °C to assess the pyrolysis operating conditions.

Following the procedure described in a previous study [50], thermal cracking of the digestate was carried out in a semi-batch reactor under atmospheric pressure and an inert atmosphere of argon. The pyrolysis was carried out in an R-101 reactor, an autoclave stirred reactor with a volume of 500 mL. For each cracking experiment, approximately 20 g of digestate was added to the reactor, which was heated from room temperature to 400 °C at an average heating rate of 10 °C/min. the experiment were performed four times. After pyrolysis, the resulting biochar was ground in a mechanical mortar and sieved to less than 45 µm.

Biochar Particle Characterization

The size of the biochar particles was measured using a Malvern Mastersizer 2000 granulometer. The Mastersizer 2000 granulometer was equipped with a Malvern Hydro 2000 MU, which uses a stirrer to disperse 1 g of sample in 800 mL of deionised water. All analyses were performed at two different stirrer speeds of 2000 and 3000 rpm after 5 min of sonication. The diameter size distribution was plotted after measurements on six different samples. The particle distribution curves were extrapolated from this measurement. Three factors were calculated, d10, d50 and d90, representing the maximum diameter value of 10%, 50% and 90% of the particles respectively.

In order to understand the chemical composition, ATR-FTIR analysis was carried out on the BC (Perkin-Elmer

FT-IR/NIR Spectrum 400, Waltham, MA, USA) and 8 acquisitions were made for each measurement.

Particle morphology was analysed by scanning electron microscopy (SEM) (Quanta 200 F ESEM, FEI, Hillsboro, USA). All samples were sputter-coated with a thin layer of gold to avoid electrostatic charging under the electron beam. Energy dispersive X-ray (EDX) analysis was also performed on the particles.

Biocomposites Formulation

Prior to processing, biopolymer pellets and BC particles were dried at 60 °C under vacuum to avoid hydrolysis phenomena, then the biocomposite formulation was carried out using a batch mixer (Brabender model PLE330, Duisburg, Germany) at 170 °C with a mixing speed of 50 rpm for 5 min, with simultaneous addition of BC and polymer matrix. Sample codes with relative polymer and filler concentrations are described in Table 1. To characterise the biocomposites, pellets of all materials were dried in a vacuum oven under the same conditions as above and then compression moulded using a Carver Laboratory Press, (Carver, Wabash; IN; USA) at a temperature of 170 °C at 300 psi for about 3 min.

Biocomposites Characterization

Rheological tests were performed using a strain-controlled rheometer (mod. ARES G2 from TA Instrument, New Castle, DE, USA) in parallel plate geometry (plate diameter 25 mm). The complex viscosity (η^*) and storage (G') and loss (G'') moduli were measured by performing frequency scans from $\omega = 10^{-2}$ to 10^2 rad/s at the same processing temperatures. The strain amplitude was $\gamma = 5\%$, which preliminary strain sweep experiments showed to be low enough to be in the linear viscoelastic regime.

A scanning electron microscope (SEM, Quanta 200 ESEM, FEI, Hillsboro, OR, USA) was used to examine the microstructure of the biocomposites. Prior to SEM analysis, the samples were fractured in liquid nitrogen. The fractured surface of each sample was sputtered (Scancoat Six Edwards, Crawley, UK) with a thin layer of gold under an argon atmosphere for 90 s to avoid electrostatic charging under the electron beam. The particle size distribution curve

of BC particles after processing was measured on the SEM micrographs using image processing software freely available from the National Institute of Health USA (ImageJ, Bethesda, MD, USA).

Tensile tests were performed on seven rectangular specimens using a universal testing machine (Instron model 3365, Rochdale, UK) according to ASTM D638-14. The tests were performed at a tensile speed of 1 mm/min for 1 min to evaluate the Young's modulus, and then the speed was increased to 10 mm/min until the specimen broke. The average values for elongation at break, EB, modulus of elasticity, E, and tensile strength, TS, were calculated.

Dynamic mechanical thermal tests (DMTA) were carried out in tensile configuration through a dynamic mechanical analyser model DMA + 50 (Metravib, Limonest, France). The test was performed on three specimens (10 mm × 30 mm) of each composite from room temperature to 140 °C at a heating rate of 5 °C/min. The frequency was set at 1 Hz and the dynamic displacement was set at 5×10^{-5} m.

The intrinsic viscosity η was measured using an iVise LMV 830 capillary viscometer (Lauda Proline PV 15, Lauda-Königshofen, Germany) equipped with a Ubbelohde ($K = 0.005$) capillary viscometer in an oil bath thermostated at 27 °C. To prepare the solution at a concentration of 0.2 wt%, each material was dissolved in tetrahydrofuran (THF) with stirring at 50 °C for 1 h. To evaluate the intrinsic viscosity of the composites, each composite was dissolved in THF, the solid fraction was removed with filter paper, the resulting solution was poured and a 0.2 wt% solution was prepared. Flow time measurements were performed in triplicate for each sample until the standard deviation was less than 0.5 s. The intrinsic viscosity values were calculated according to Solomon-Ciuta using the equation [53]:

$$[\eta] = \frac{\sqrt{2}}{c} \sqrt{\eta_{sp} - \ln \eta_{rel}}$$

where c is the concentration of the polymer solution, η , η_{sp} and η_{rel} are the intrinsic, specific and relative viscosities, respectively. The solution viscosity of each sample was obtained by averaging 5 flow measurements. The viscosimetric molecular weight (M_v) was calculated using the Mark-Houwink equation:

Table 1 Sample code name with relative weight concentration

Sample	PBAT [wt%]	PLA [wt%]	Sample	PBAT [wt%]	PLA [wt%]	BC [wt%]
PBAT:PLA 100:0	100	0	PBAT:PLA/BC 100:0/10	90	0	10
PBAT:PLA 75:25	75	25	PBAT:PLA/BC 75:25/10	67.5	22.5	10
PBAT:PLA 50:50	50	50	PBAT:PLA/BC 50:50/10	45	45	10
PBAT:PLA 25:75	25	75	PBAT:PLA/BC 25:75/10	22.5	67.5	10
PBAT:PLA 0:100	0	100	PBAT:PLA/BC 0:100/10	0	90	10

$$[\eta] = KM_v^a$$

Depending on the specific polymer-solvent system, the parameter values of the Mark-Houwink constants, a and K , are different. For PLA-THF, $K = 1.74 \cdot 10^{-4}$ and $a = 0.736$ [54]. For PBAT-THF, $K = 1.5 \cdot 10^{-4}$ and $a = 0.766$ [55].

Results and Discussion

Digestate and Biochar Analysis

Prior to the pyrolysis process, the digestate was characterised by thermogravimetric analysis to investigate the thermal degradation path of the waste. Figure 1 shows that digestate degradation at low heating rates occurs over a wide temperature range, which narrows as the heating rate increases. The derivative thermogravimetric (DTG) curves show four different, well-differentiated peaks, suggesting a complex degradation pathway of the digestate waste, which takes place through four different degradation steps. In fact, referring to the DTG curve with a heating rate of $10^\circ\text{C}/\text{min}$, the first DTG peak at about 104.31°C is related to the removal of moisture content and very high volatile components. Furthermore, the other three peaks can be considered as degradation peaks of a lignocellulosic feedstock. This assumption may be reasonable since digestate is derived from the anaerobic digestion of organic matter. Thus, according to the literature, biomass degradation after thermal stress is essentially in three steps: (i) hemicellulose degradation, (ii) lignin and cellulose degradation, and (iii) lignin decomposition [56]. Thus, at a heating rate of $10^\circ\text{C}/\text{min}$, the digestate shows that hemicellulose degradation occurs at 214.78°C ,

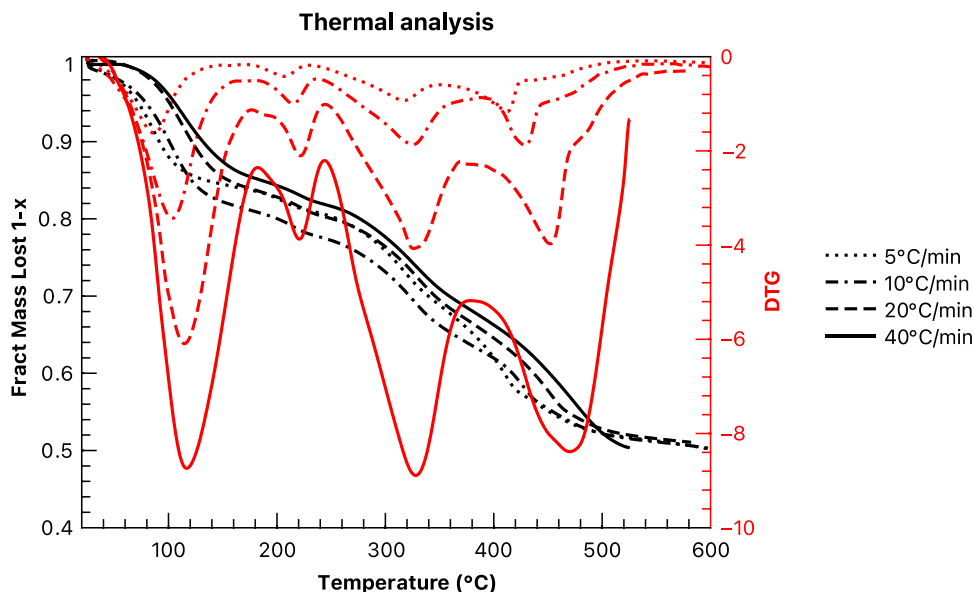
while lignin and cellulose degradation and lignin decomposition occur at 326.71 and 429.92°C , respectively. In accordance with the DTG curves and a previous study [40], a temperature of 400°C was chosen to pyrolyse the waste as a compromise between the need for weight loss and the need to save energy compared to 429.92°C .

Before using biochar as a filler for PBAT:PLA blends, it was ground with a mechanical pestle and mortar and sieved to less than $45\ \mu\text{m}$. The final size of the BC particles was measured using an ultrasonic granulometer equipped with a dispersant unit able to use different stirrer speeds. The stirring speeds, in fact, affects the homogenisation of the particles in solution, and thus the final particles size distribution (PSD) curves, resulting slight difference between Fig. 2a and b. It gives more confidence in the measurement to report that the error is small at both speeds.

According also to the SEM morphology (see Fig. 3a, b), almost all the particles have a diameter less than $100\ \mu\text{m}$: thanks to the d_{10} factor, it is possible to state that at least 10 v.% of the particles have a diameter less than $5\ \mu\text{m}$, with many particles less than $1\ \mu\text{m}$ (Fig. 3a) which, after sonication during the Mastersizer measurement, break up from agglomerates to be led in solution. The sieving process was efficient: the maximum of the particle size distribution curves varies from $52.1\ \mu\text{m}$ to $35.4\ \mu\text{m}$ by varying the stirring speed during the measurements from 2000 to 3000 rpm, and certainly 90% of the particles have a diameter smaller than $87.2\ \mu\text{m}$.

In order to chemically characterise the biochar, ATR-FTIR analysis of the BC was carried out (see Fig. 3c) and compared with the digestate prior to pyrolysis, and EDX measurements were carried out (see Fig. 4). The ATR-FTIR spectra show a reduction of several

Fig. 1 TG and DTG Curves of Digestate at different heating rate



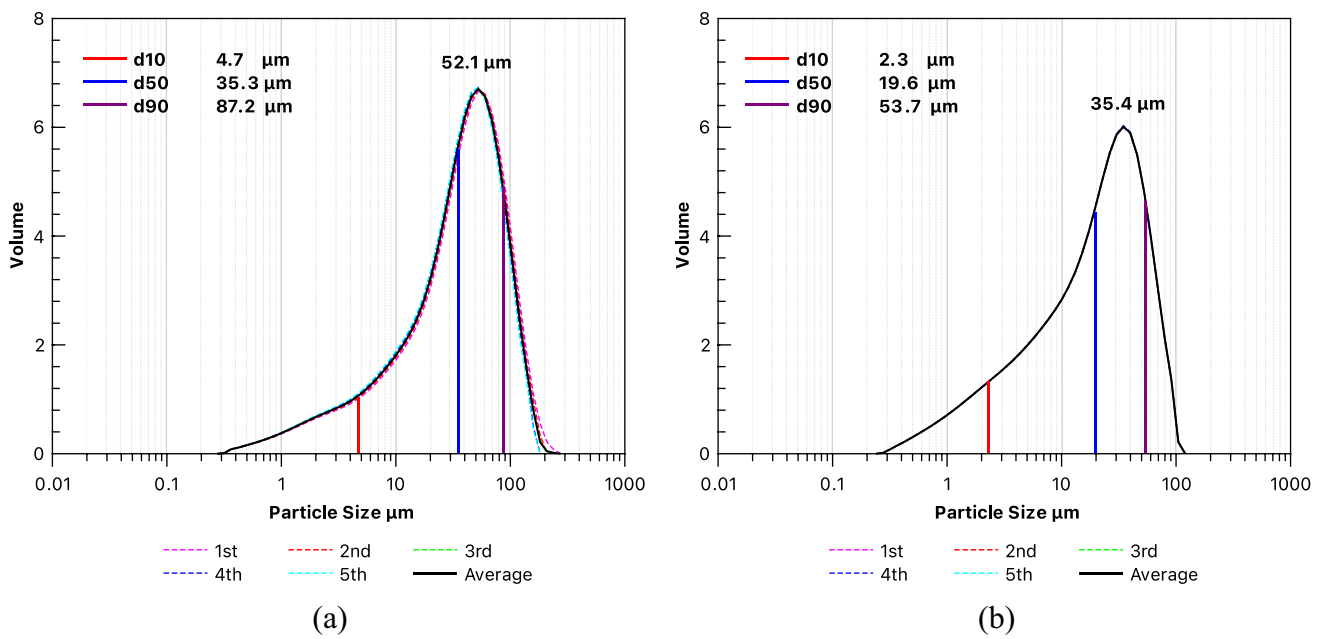


Fig. 2 Particles-size distribution curves at different stirring velocity **a** 2000 and **b** 3000 rpm

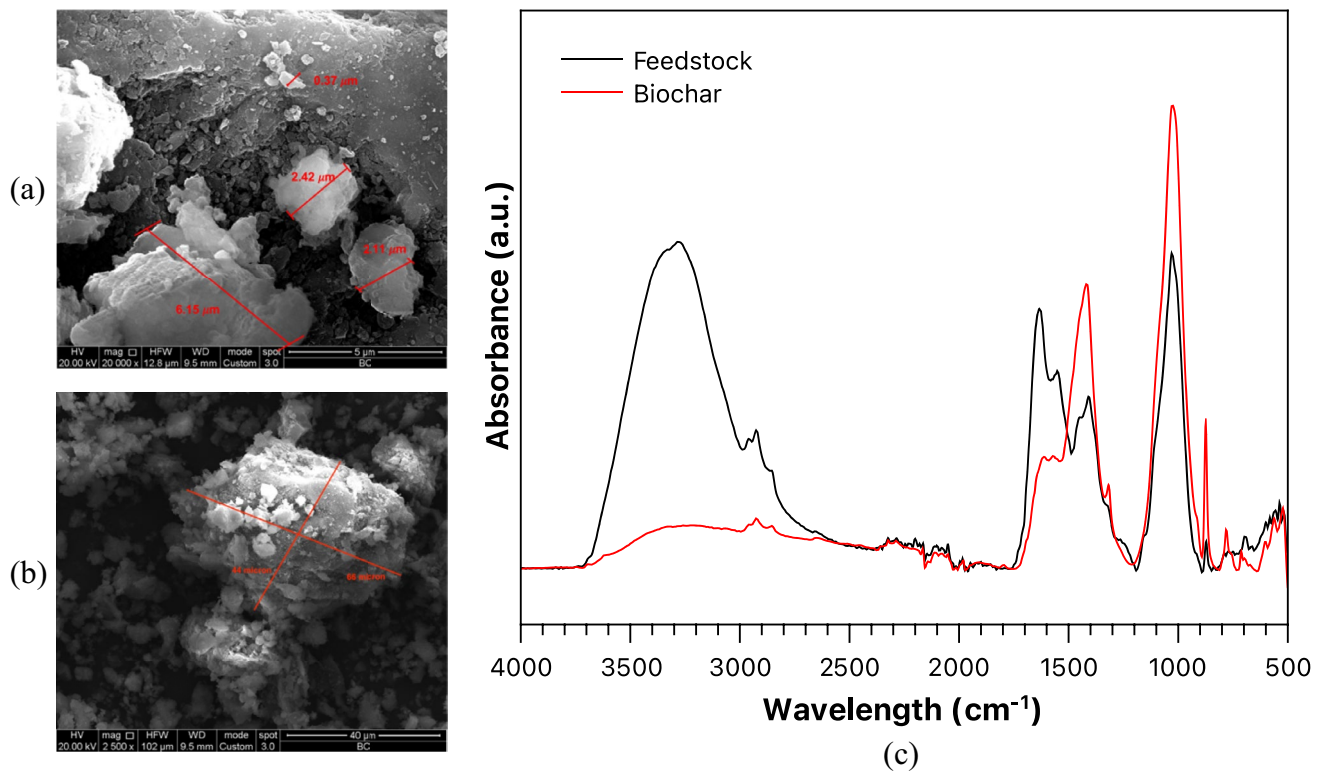


Fig. 3 SEM morphologies of biochar at **a** 20 000 x and **b** 2 500 x and **c** ATR-FTIR spectra of digestate before pyrolysis and resulting biochar

characteristic lignocellulosic bands, for example: the broad band between 3300 and 3600 cm^{-1} with a maximum at 3288 cm^{-1} (ν_{OH} , OH stretching vibrations of

hydrogen-bonded hydroxyl groups), the two peaks at 2920 and 2948 cm^{-1} (asymmetric and symmetric CH stretching vibrations of aliphatic groups), the peak at 1628 cm^{-1}

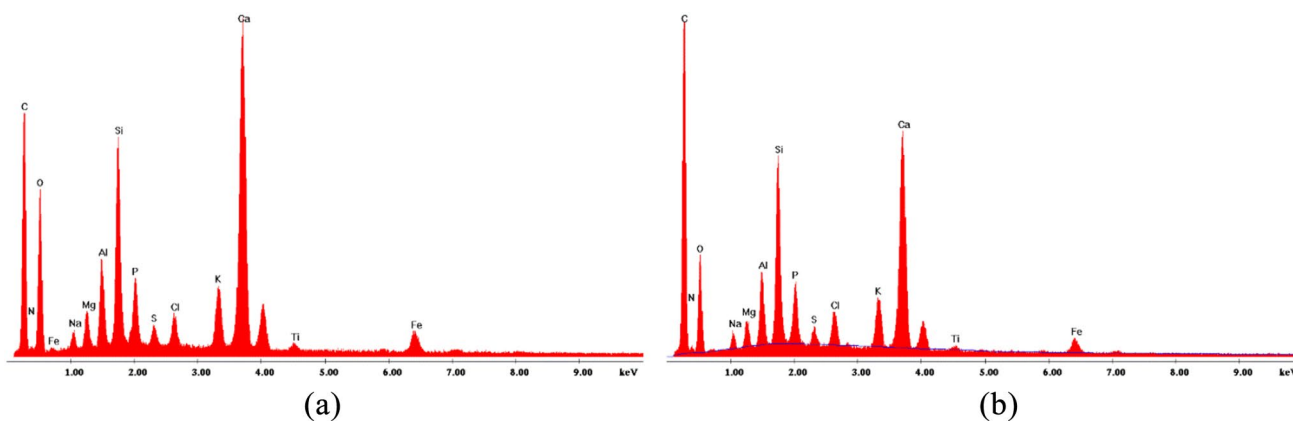


Fig. 4 EDX spectra of biochar obtained by slow pyrolysis of digestate at 400 °C and 1 atm at different magnitudes: (a) 50 x and (b) 1000 x

(related to aromatic C=C stretching and C=O stretching modes). Thermal cracking is responsible for breaking chemical bonds to rearrange them into new functional groups. The reduction of hydrogen-bonded hydroxyl groups, aliphatic groups, and C=C and C=O aromatic groups (which appears to be partial rather than complete) can be attributed to incomplete thermal degradation of the feedstock. As stated before, at 400 °C, hemicellulose, cellulose and some lignin degradation occurred. The rearrangement of these chemical structures as a result of the pyrolysis process can be seen by the increase in certain bands, such as: the peak at 1420 cm^{-1} , related to aromatic structural vibrations, the peak at 1026 cm^{-1} , normally related to C–O stretching, the two peaks at 876 and 778 cm^{-1} , related to aromatic C–H deformation modes [57–59].

In addition, EDX analysis was carried out to characterise the elemental composition of the BC surface at two different magnifications: 50x and 1000x to evaluate the elemental concentration of BC qualitatively and quantitatively. The sample results are homogeneous, although some element concentrations differ by a few percentage points. However, all atoms with an atomic weight lower than sodium have an intrinsic error in weight determination. Nevertheless, as shown in Fig. 4, several elements have been detected by EDX spectroscopy: from carbon to iron and titanium. It can be stated that BC is mainly composed of carbon and oxygen. Other elements with significant concentrations are: aluminium, silica, phosphorus, potassium and calcium. In this study, for the characterisation of the composites, it is important to highlight the presence of iron in low concentration [60–62]. The high variety and quantity of inorganic contents are attributed to the inhomogeneity of OFMSW and its inorganic components, such as bones and table salt, present in the initial food waste.

Composites

The complex viscosity as a function of angular frequency of bio-blend and bio-composites is shown in Fig. 5. In Fig. 5a, the curves show that the original samples (PBAT:PLA 0:100 and PBAT:PLA 100:0) have the same complex viscosity at low frequency, with a more Newtonian behaviour for pure PLA compared to pure PBAT. In fact PBAT shows a more pronounced decrease in complex viscosity with increasing angular frequency. In fact, unlike PLA, PBAT shows a narrower Newtonian range, exhibiting a shear-thinning behaviour already from 1 rad/s to higher angular frequency tested. Accordingly, in blend formulation, the addition of PBAT limits the Newtonian range, with the shear thinning tendency becoming more pronounced with increasing PBAT content. For blends with a predominance of one of the two matrices (PBAT:PLA 75:25 and PBAT:PLA 25:75), the complex viscosity at low frequency is higher than that of the pure matrix, with the appearance of a stress-strain behaviour at low frequency, suggesting a change in morphology. However, PBAT:PLA 50:50 shows a more balanced behaviour between the two matrices. This phenomenon is classical for immiscible polymer blends and depends on the higher shear that occurs between the two phases. In fact, for immiscible polymers, the formation of droplets of the minor phase in the major phase results in an increase of the complex viscosity. For the blend in which PBAT and PLA are equivalent, as visible later in the morphology section, no droplet formation is visible and the morphology results in an elongated co-continuous phase that result responsible of an easier sliding of the polymer chain under shear [63, 64]. Thus, the blends have a higher complex viscosity at low frequency and a pronounced shear thinning behaviour during the frequency range, suggesting a high interaction between the two matrices [5, 24], with a decrease in complex viscosity

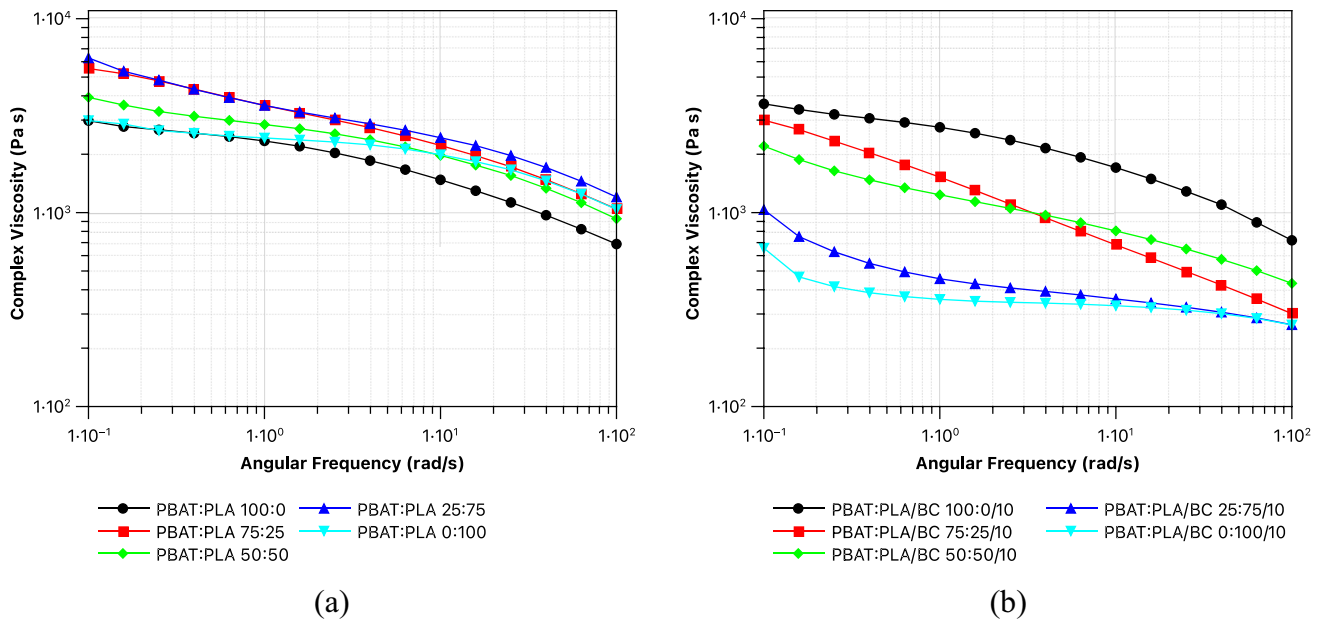


Fig. 5 Complex Viscosity versus angular frequency for different PBAT:PLA blend composition **a** without and **b** with 10 wt.% of BC particles

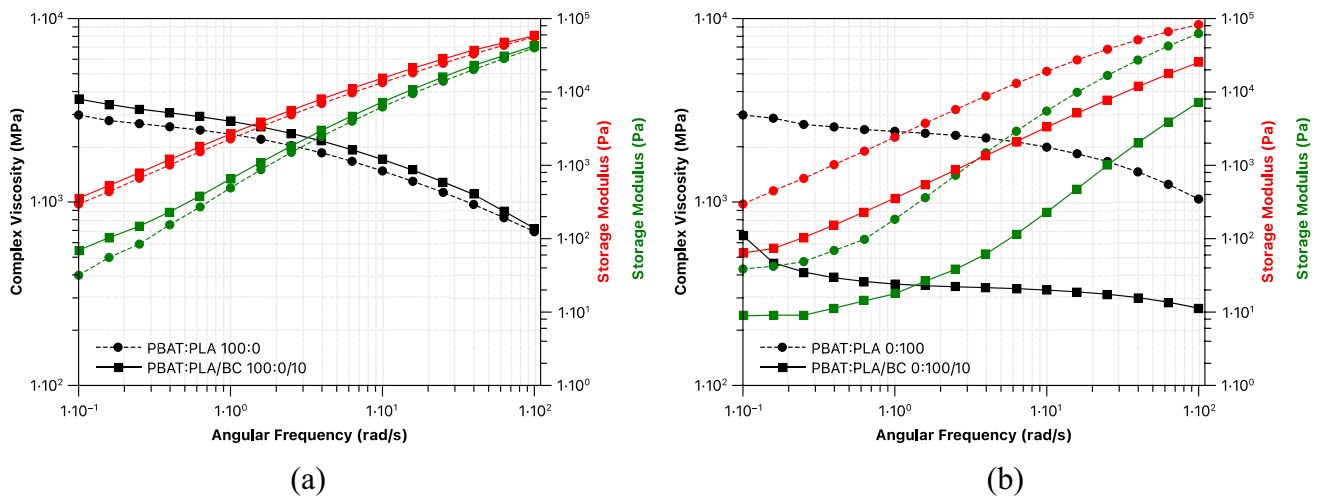


Fig. 6 Rheological behaviour of **a** PBAT:PLA 100:0 with and without 10 wt.% of BC **b** PBAT:PLA 0:100 with and without 10 wt.% of BC

at higher frequency due to disentanglement of the molecular chain [19, 25].

As shown in Fig. 6, the addition of 10 wt% BC to virgin PBAT or virgin PLA determines two different rheological behaviours. In fact, as seen in the previous study [40], 10 wt% BC on PBAT matrix determines a global increase of the complex viscosity, as shown in Fig. 6a. Differently, as shown in Fig. 6b, for pure PLA the addition of 10 wt% BC completely modifies the rheological behaviour with a significant reduction of the complex viscosity and a stress-strain behaviour at low frequency. This behaviour

is usually seen when a plasticiser is added to a polymer matrix or degradation phenomena occur.

Turning to the study of the composite blends, the rheological behaviour depends on the weight ratio between PBAT:PLA to mean the balance between their two antithetic behaviours. Figure 5b shows the rheological behaviour of composite blends compared to PBAT and PLA based composites. At low frequency, the complex viscosity decreases as the PLA content in the blend increases, similar to that of the PLA composite. The presence of BC particles and their interaction with the polymer blend is more visible in the

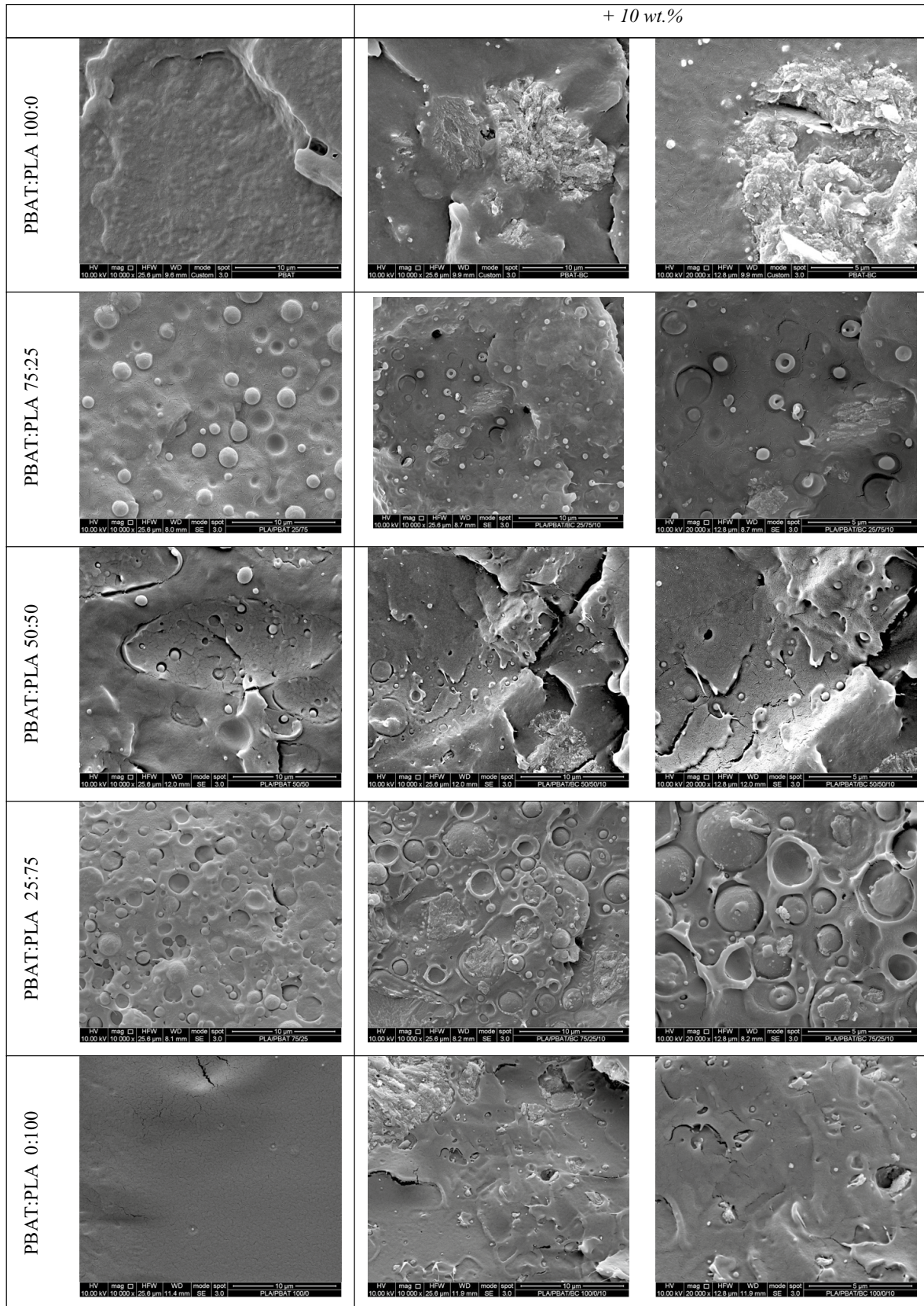


Fig. 7 SEM images of blend varying PBAT:PLA weight ratio, with and without 10 wt.% of BC

stress-strain behaviour at low frequency when the amount of PLA exceeds the amount of PBAT in the biopolymer blend. Instead, the PBAT:PLA/BC 75:25/10 complex viscosity has a more pronounced angular frequency dependence. The PBAT:PLA/BC 50:50/10 showed both stress-yield behaviour and a pronounced decrease in complex viscosity with increasing angular frequency.

Figure 7 shows the SEM images of the nitrogen-fractured surface for the PBAT:PLA blends with different composition ratios, showing a typical two-phase structure. In accordance with the rheological behaviour, the morphology changes with increasing PLA content in the PBAT:PLA blend. As shown in the first column of Fig. 7, the morphology changes from spherical droplets (PBAT:PLA 75:25) to a co-continuous elongated structure (PBAT:PLA 50:50) and back to spherical droplets [23, 65]. In composite SEM images, the average size of BC particles in biopolymer blends appears to be smaller than the dimension shown in Fig. 3c (see Figures S1 and S2 in Supplementary Information). This phenomenon is probably due to the shear stress experienced by BC during melt mixing, which also favours a deagglomeration of smaller particles seen in Fig. 3b, which appear homogeneous and well dispersed in the biopolymer blend.

The reduction in particle size that occurred during melt mixing could cause an increase in the polymer/filler interface area, with a consequent increase in the interaction between BC and the biopolymer blend. Also in this case, and in accordance with the rheological behaviour, this interaction led to a change in morphology depending on the PBAT:PLA weight ratio. Concerning the addition of BC to pristine PBAT matrix, a good adhesion and dispersion between biopolymer matrix and BC particles was shown, as already reported in a previous study [40]. When added to pristine PLA matrix, good dispersion is achieved, but a dissection between polymer matrix and BC occurs, with clear gaps surrounding BC particles. Moreover, in the presence of BC, when PLA is the minor phase (PBAT:PLA/BC 75:25/10), its droplets homogeneously distributed in the PBAT matrix change from spherical shape to “donut” shape, with a global reduction of the mean particle diameter. Conversely, when PBAT is the minor phase (PBAT:PLA/BC 25:75/10), the homogeneously distributed PBAT droplet retains the spherical shape. In this case, the major phase of PLA changes its morphology and shows a “volcano” shape around the PBAT droplet. For PBAT:PLA/BC 50:50/10, a co-continuous elongated structure appears to be preserved, although the PLA appears slightly damaged.

Figure 8 shows the mechanical properties of the blends, namely Young's modulus, tensile strength and elongation at break. As expected, for the blend without BC (black line), a transition from a rigid material to a ductile material is observed with increasing PBAT wt%, from a higher young modulus and lower elongation at break values for

pure PLA to a lower young modulus and higher elongation at break values for pure PBAT. In line with the rheological behaviour and morphology, the presence of BC has (i) a reinforcing role for PBAT that, as it is aspect, moves the mechanical behaviour of PBAT from ductile to rigid, and (ii) a reduction in mechanical properties for PLA. Consequently, for the blend composition, when PBAT is the main phase, BC shows a small reinforcing role, while when PLA is the main phase, biocomposites show a reduction in mechanical properties. Nevertheless, for PBAT:PLA/BC 50:50/10, an increase in Young's modulus, tensile strength occurs without much variation in elongation at break, probably due to the preservation of the co-continuous elongated morphology and a good dispersion of BC in the blend.

The results of the DMA analysis are shown in Fig. 9 as the variation of the logarithm of the storage moduli and the damping factor with temperature. The storage modulus E' and the damping factor ($\tan\delta$) for the blend and the blend filled with 10 wt.% BC as a function of temperature are shown in Fig. 9, from room temperature to 140°C, where possible. As expected, the first observation is related to the differences in the storage modulus at room temperature and in the shape of the storage modulus curve between the pure PBAT and the blend with PBAT in the major concentration with respect to the pure PLA and the blend with PLA in the major concentration. Instead, for the PBAT:PLA 50:50 blend, the mechanical behaviour of PLA prevails, with a storage modulus at room temperature comparable to that of pure PLA and a pronounced increase in E' (with a maximum at $\approx 130^\circ\text{C}$) due to the cold crystallisation phenomena of PLA. A second observation is related to the shape of the damping factor curve: the main peak at $\tan\delta$ is related to the T_g of PLA, since that of PBAT is normally observed around between 30 and -20°C . In Fig. 9b it is clear how the T_g of PLA in the blend remains constant and equal to $70.3 \pm 0.6^\circ\text{C}$, and the increase in magnitude results coherent with the increase of PLA in the blend: namely PBAT, the rubbery phase, acts as a stress concentrator. When the blends are filled with 10 wt.% BC, the first observation is the shift towards a lower value of E' of the PBAT:PLA/BC 75:25/10 and PBAT:PLA/BC 50:50/10 blends, coherent with the tensile properties already shown. The storage moduli below the glass transition temperature of PLA are lower for all PBAT:PLA weight ratios, except for pure PBAT. This behaviour is consistent with the tensile properties and rheological behaviour. Moreover, a different shape with a double shoulder in the E' curves, caused by PLA cold crystallisation phenomena. As regards the damping factor, a significant reduction in the size of the main peaks related to T_g is observed, indicating a low damping capacity in the presence of BC. Furthermore, a shift towards a lower value of T_g is observed with the increase of PLA in the blend, from 71.4°C for PBAT:PLA/BC 75:25/10 to a T_g of 66.4°C for

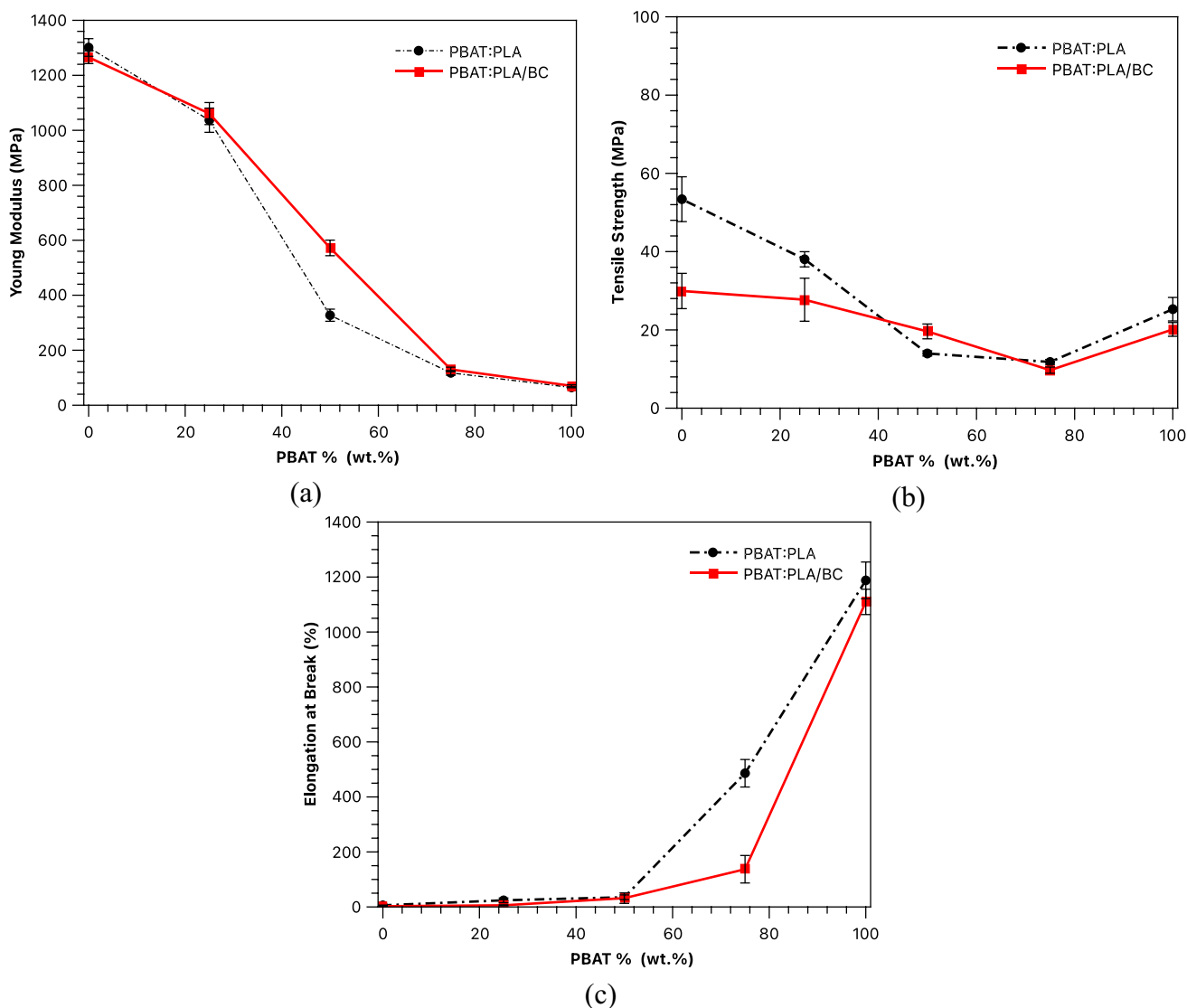


Fig. 8 Mechanical properties of PBAT:PLA blend with and without BC as a function of PBAT content

PBAT:PLA/BC 25:75/10. The slight decrease in glass transition temperature with increasing PLA in the biocomposite blend and the decrease in peak size is consistent with the behaviour observed with rheological analysis. We hypothesize that the decrease in storage moduli below the glass transition temperature and the decrease in T_g are due to a possible degradation of the PLA polymer chain, caused by the presence of BC in the blend [38].

In order to evaluate the degradation phenomena likely to be suggested by the previous characterisation, a measurement of the molecular weight was carried out by means of intrinsic viscosity measurements and correlated to the molecular weight M_v by means of Mark-Houwink constants. Table 2 shows the results of the capillary viscosimetry carried out on PBAT and PLA, with and without 10 wt% BC. The viscous molar mass of the biocomposites

was compared with that of the pure matrix subjected to the same process condition. The table shows that M_v of PBAT processed in the presence and in absence of BC keeps its viscous molecular weight constant. Indeed, the dimensionless value of the viscous molar mass is close to one. While for PLA a significant reduction of the viscous molar mass has been highlighted, in fact the dimensionless molar mass results 0.5. For PBAT, the loading of BC as a reinforcing filler leads to an increase in mechanical and rheological properties. Instead, the reduction in viscosity and molar mass of PLA suggests a scission of the molecular chains induced by the presence of BC in the composite. This result is probably due to the fact that BC causes or accelerates the degradation of PLA, thereby reducing the molar mass [39, 66]. As stated before some traces of iron were found on the surface of the BC, and it has been

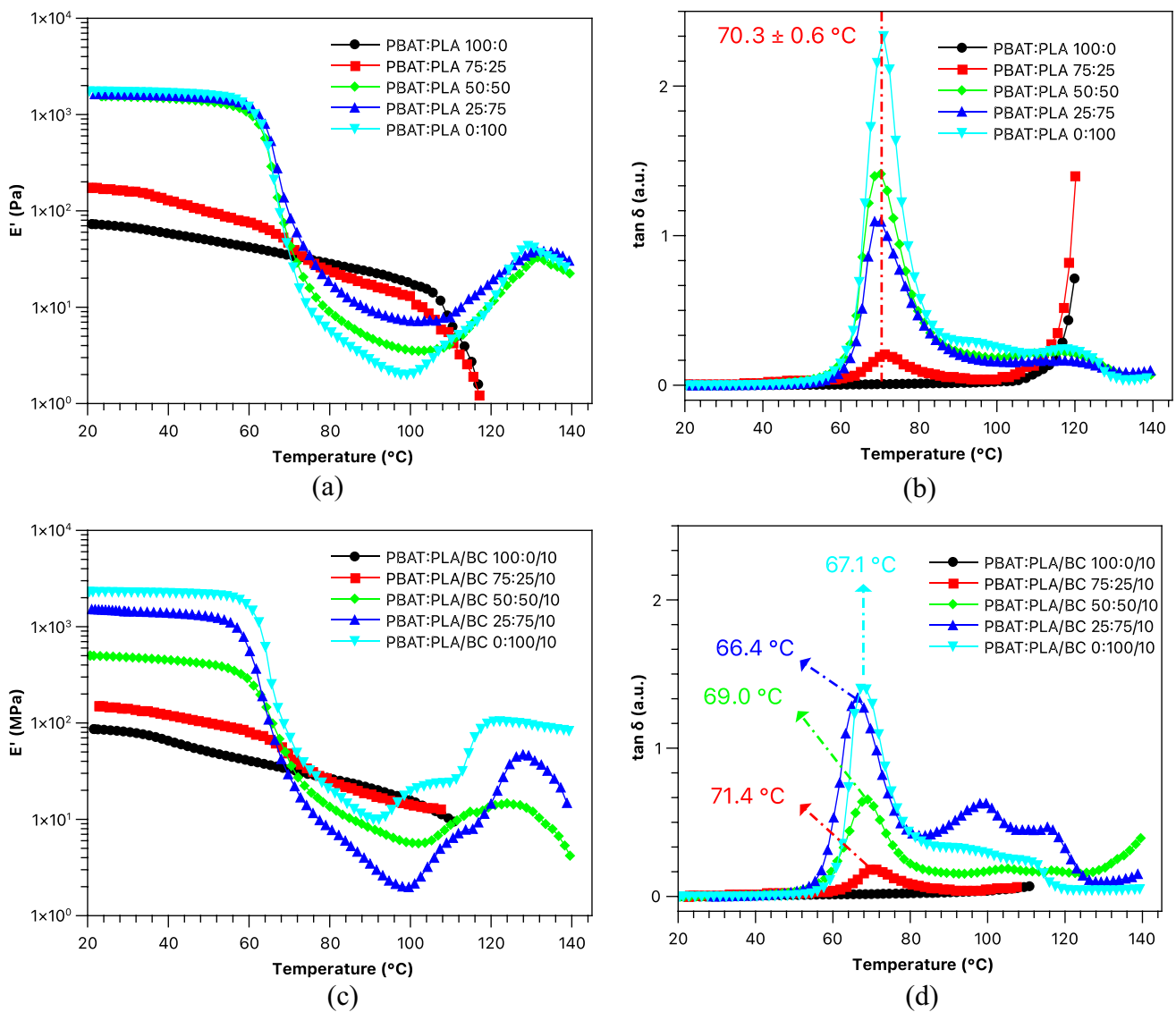


Fig. 9 Storage modulus and damping factor graphs for biopolymer blend **a,b** without and **c,d** with 10 wt.% of BC

Table 2 Viscous molar mass, intrinsic viscosity, and dimensionless values of molar mass of PBAT and PLA with and without 10 wt% of BC

	M_v^0 [g/mol]	η_i [dL/g]		M_v [g/mol]	η_i [dL/g]	$\frac{M_v}{M_{v0}}$ [-]
PBAT:PLA 100:0	5.32×10^4	0.63	PBAT:PLA/BC 100:0/10	5.79×10^4	0.67	1.08
PBAT:PLA 0:100	1.58×10^5	1.17	PBAT:PLA/BC 0:100/10	7.91×10^4	0.7	0.50

suggested from the literature that Fe^{3+} could react with carbonyl oxygen and the adjacent carbon to form stable Fe–O and Fe–C chemical bonds, which are able to weaken the ester bond of PLA [67]. In addition, the possibility that the presence of inorganic materials may catalyze the thermal decomposition of PLA has recently been demonstrated by Kane et al. [43].

Conclusion

In this work, a fully biodegradable biopolymer blend based on PBAT and PLA matrices was prepared by varying the weight ratio between the two biopolymer matrices. The biochar added to the different biopolymer blends was

obtained in our laboratories using digestate as a feedstock. Initially, the digestate was thermally characterised to evaluate the pyrolysis temperature condition. The dimensional and chemical characterisation highlighted a maximum diameter of BC particles of 45 μm and a high carbon content, with residual inorganic and metal atoms on the surface of BC particles. For biocomposites blend rheological behaviour, the addition of BC modifies complex viscosity depending particularly on PLA interaction with BC particles, and consequently on the increase of PLA matrix in polymer blend. From the mechanical characterisation of the filled blend, it is evident that degradation phenomena occur caused by the interaction between PLA and BC particles. From the morphological characterisation, it is clear how different is the interaction between BC particles and the two different polymer matrices, showing an overall good BC dispersion in the polymer matrix, even if a better interfacial adhesion was highlighted in the presence of PBAT matrix, and some degradative evidence was found on PLA matrix. Thus, the rheological, morphological and mechanical behaviour of BC filled blends highlight the challenges of using BC particles as filler for PLA or PLA based blends. Indeed, degradation phenomena when BC interacts with the PLA matrix have been confirmed by means of a capillary viscosimeter, evaluating the viscous molar mass of the two polymers matrix processed in the absence and in the presence of BC particles. In fact, a significant reduction in the molecular weight of PLA is probably due to a strong interaction between PLA and the residual inorganic elements present on the BC surface after pyrolysis. In short, the excellent properties of BC particles obtained from digestate pyrolysis could certainly be used as a filler for biopolymer blends, although the composition of the blend is a determining factor.

Supplementary Information The online version contains supplementary material available at <https://doi.org/10.1007/s10924-023-03108-1>.

Author Contributions GI: Investigation, Data curation, Writing—original draft preparation, Writing—review & editing. LB: Conceptualization, Investigation, Methodology, Writing—Review & Editing, Supervision, Funding acquisition. II: Investigation. MM: Investigation, Data curation. GC: Data curation, Methodology, Writing—Review & Editing, Funding acquisition. NTD: Data curation, Visualization, Writing—Review & Editing, Supervision.

Funding Open access funding provided by Università degli Studi di Palermo within the CRUI-CARE Agreement. This work was supported: by the Italian Programma Operativo Nazionale (PON): PON BIOFEEDSTOCK ARS01_00985.

Data Availability Data will be made available on request.

Declarations

Competing Interests The authors have no competing interests to declare that are relevant to the content of this article.

Open Access This article is licensed under a Creative Commons Attribution 4.0 International License, which permits use, sharing, adaptation, distribution and reproduction in any medium or format, as long as you give appropriate credit to the original author(s) and the source, provide a link to the Creative Commons licence, and indicate if changes were made. The images or other third party material in this article are included in the article's Creative Commons licence, unless indicated otherwise in a credit line to the material. If material is not included in the article's Creative Commons licence and your intended use is not permitted by statutory regulation or exceeds the permitted use, you will need to obtain permission directly from the copyright holder. To view a copy of this licence, visit <http://creativecommons.org/licenses/by/4.0/>.

References

1. European Commission (2018) Communication from the commission to the European Parliament, the council, the european economic and social committee and the committee of the regions Closing the Loop -An EU action plan for the circular economy. Brussels.
2. Auras R, Harte B, Selke S (2004) An overview of polylactides as packaging materials. *Macromol Biosci* 4:835–864. <https://doi.org/10.1002/mabi.200400043>
3. Babu RP, O'Connor K, Seeram R (2013) Current Progress on Bio-Based Polymers and Their Future Trends. *Prog Biomater* 2:1. <https://doi.org/10.1186/2194-0517-2-8>
4. Jian J, Xiangbin Z, Xianbo H (2020) An overview on synthesis, Properties and Applications of Poly(Butylene-Adipate-Co-Terephthalate)–PBAT. *Adv Ind Eng Polym Res* 3:19–26. <https://doi.org/10.1016/j.aiepr.2020.01.001>
5. Moustafa H, El Kissi N, Abou-Kandil AI, Abdel-Aziz MS, Dufresne (2017) A. PLA/PBAT bionanocomposites with Antimicrobial Natural Rosin for Green Packaging. *ACS Appl Mater Interfaces* 9:20132–20141. <https://doi.org/10.1021/acsami.7b05557>
6. Moustafa H, Guizani C, Dupont C, Martin V, Jeguirim M, Dufresne A (2017) Utilization of Torrefied Coffee Grounds as reinforcing Agent to produce high-quality biodegradable PBAT composites for Food Packaging Applications. *ACS Sustain Chem Eng* 5:1906–1916. <https://doi.org/10.1021/acssuschemeng.6b02633>
7. Murariu M, Laoutid F, Dubois P, Fontaine G, Bourbigot S, Devaux E, Campagne C, Ferreira M, SolarSKI S (2014) Pathways to biodegradable flame retardant polymer (nano) composites. *Polymer green flame retardants*. Elsevier, Amsterdam, pp 709–773
8. Infurna G, Cavallaro G, Lazzara G, Milioto S, Dintcheva NT (2021) Understanding the effects of crosslinking and reinforcement agents on the performance and durability of biopolymer films for cultural heritage protection. *Molecules* 26:3468. <https://doi.org/10.3390/molecules26113468>
9. Luckachan GE, Pillai CKS (2011) Biodegradable Polymers- A review on recent trends and emerging perspectives. *J Polym Environ* 19:637–676. <https://doi.org/10.1007/s10924-011-0317-1>
10. Notta-Cuvier D, Murariu M, Odent J, Delille R, Bouzouita A, Raquez J-M, Lauro F, Dubois P (2015) Tailoring polylactide properties for automotive applications: effects of co-addition of halloysite nanotubes and selected plasticizer. *Macromol Mater Eng* 300:684–698. <https://doi.org/10.1002/mame.201500032>
11. Notta-Cuvier D, Odent J, Delille R, Murariu M, Lauro F, Raquez JM, Bennani B, Dubois P (2014) Tailoring polylactide (PLA) Properties for Automotive Applications: effect of addition of

- designed additives on Main Mechanical properties. *Polym Test* 36:1–9. <https://doi.org/10.1016/j.polymertesting.2014.03.007>
12. Pawar P, Tekale R;U, Shisodia S;U, Totre S;T, Domb J;J (2014) Biomedical Applications of Poly(Lactic Acid). *Recent Pat Regen Med* 4:40–51. <https://doi.org/10.2174/2210296504666140402235024>
 13. Sin LT, Rahmat AR, Rahman WAWA (2013) Applications of poly(lactic acid). *Handbook of biopolymers and biodegradable plastics*. Elsevier, Amsterdam, pp 55–69
 14. Niaounakis M (2013) Economic evaluation and environmental impacts. *Biopolymers reuse, recycling, and disposal*. Elsevier, Amsterdam, pp 275–290
 15. Datta R, Henry ML, Acid (2006) Recent advances in products, processes and technologies — a review. *J Chem Technol Biotechnol* 81:1119–1129. <https://doi.org/10.1002/jctb.1486>
 16. Middleton JC, Tipton AJ (2000) Synthetic biodegradable polymers as Orthopedic devices. *Biomaterials* 21:2335–2346. [https://doi.org/10.1016/S0142-9612\(00\)00101-0](https://doi.org/10.1016/S0142-9612(00)00101-0)
 17. Perepelkin KE (2002) Polylactide fibres: fabrication, properties, use, prospects. A review. *Fibre Chem* 34:85
 18. Witt U, Einig T, Yamamoto M, Kleeberg I (2001) Biodegradation of aliphatic–aromatic copolyesters: evaluation of the final biodegradability and ecotoxicological impact of degradation intermediates. *Chemosphere* 44:289
 19. Deng Y, Yu C, Wongwiwattana P, Thomas NL (2018) Optimising ductility of poly(lactic acid)/Poly(Butylene Adipate-Co-Terephthalate) blends through co-continuous phase morphology. *J Polym Environ* 26:3802–3816. <https://doi.org/10.1007/s10924-018-1256-x>
 20. Burford T, Rieg W, Madbouly S (2021) Biodegradable Poly(Butylene Adipate-Co-Terephthalate) (PBAT). *Phys Sci Rev* 0:1–30. <https://doi.org/10.1515/psr-2020-0078>
 21. Herrera R, Franco L, Rodríguez-Galán A, Puiggali J (2002) Characterization and degradation behavior of poly(Butylene Adipate-Co-Terephthalate)s. *J Polym Sci Part Polym Chem* 40:4141–4157. <https://doi.org/10.1002/pola.10501>
 22. Su S (2021) Prediction of the Miscibility of PBAT/PLA blends. *Polymers* 13:2339. <https://doi.org/10.3390/polym13142339>
 23. Su S, Duhme M, Kopitzky R, Uncompatibilized PBAT/PLA, Blends (2020) Manufacturability, Miscibility and Properties. *Materials* 13:4897. <https://doi.org/10.3390/ma13214897>
 24. Pietrosanto A, Scarfato P, Di Maio L, Nobile MR, Incarnato L (2020) Evaluation of the suitability of Poly(Lactide)/Poly(butylene-Adipate-Co-Terephthalate) blown films for Chilled and Frozen Food Packaging Applications. *Polymers* 12:804. <https://doi.org/10.3390/polym12040804>
 25. Li X, Ai X, Pan H, Yang J, Gao G, Zhang H, Yang H, Dong L (2018) The morphological, mechanical, rheological, and Thermal properties of PLA/PBAT Blown films with Chain Extender. *Polym Adv Technol* 29:1706–1717. <https://doi.org/10.1002/pat.4274>
 26. Zhang T, Han W, Zhang C, Weng Y (2021) Effect of Chain Extender and light stabilizer on the Weathering Resistance of PBAT/PLA Blend films prepared by Extrusion Blowing. *Polym Degrad Stab* 183:109455. <https://doi.org/10.1016/j.polymdegradstab.2020.109455>
 27. Weng Y-X, Jin Y-J, Meng Q-Y, Wang L, Zhang M, Wang Y-Z (2013) Poly(lactic acid) (PLA), and their blend under Soil conditions. *Polym Test* 32:918–926. <https://doi.org/10.1016/j.polymertesting.2013.05.001>. Biodegradation Behavior of Poly(Butylene Adipate-Co-Terephthalate) (PBAT)
 28. Xie J, Yan Y, Fan S, Min X, Wang L, You X, Jia X, Waterhouse GIN, Wang J, Xu J (2022) Prediction model of photodegradation for PBAT/PLA mulch films: strategy to fast evaluate service life. *Environ Sci Technol* 56:9041–9051. <https://doi.org/10.1021/acs.est.2c01687>
 29. Infurna G, Caruso G, Dintcheva NT (2023) Sustainable materials containing biochar particles: a review. *Polymers* 15:343. <https://doi.org/10.3390/polym15020343>
 30. Cha JS, Park SH, Jung SC, Ryu C, Jeon JK, Shin MC, Park YK (2016) Production and utilization of Biochar: a review. *J Ind Eng Chem* 40:1–15. <https://doi.org/10.1016/j.jiec.2016.06.002>
 31. Bruun EW, Ambus P, Egsgaard H, Hauggaard-Nielsen H (2012) Effects of slow and fast pyrolysis biochar on soil C and N turnover Dynamics. *Soil Biol Biochem* 46:73–79. <https://doi.org/10.1016/j.soilbio.2011.11.019>
 32. Clough TJ, Condon LM, Kammann C, Müller C (2013) A review of Biochar and Soil Nitrogen dynamics. *Agronomy* 3:275–293. <https://doi.org/10.3390/agronomy3020275>
 33. Elleuch A, Boussetta A, Yu J, Halouani K, Li Y (2013) Experimental investigation of direct Carbon fuel cell fueled by Almond Shell Biochar: Part I. Physico-Chemical characterization of the Biochar fuel and cell performance examination. *Int J Hydrog Energy* 38:16590–16604. <https://doi.org/10.1016/j.ijhydene.2013.08.090>
 34. Jafri N, Wong WY, Doshi V, Yoon LW, Cheah KH (2018) A review on production and characterization of Biochars for Application in Direct Carbon fuel cells. *Process Saf Environ Prot* 118:152–166. <https://doi.org/10.1016/j.psep.2018.06.036>
 35. Zhang J, Zhong Z, Zhao J, Yang M, Li W, Zhang H (2012) Study on the Preparation of activated Carbon for Direct Carbon fuel cell with Oak Sawdust. *Can J Chem Eng* 90:762–768. <https://doi.org/10.1002/cjce.20549>
 36. Ahmad M, Lee SS, Dou X, Mohan D, Sung J-K, Yang JE, Ok YS (2012) Effects of Pyrolysis temperature on soybean stover- and peanut Shell-Derived Biochar properties and TCE Adsorption in Water. *Bioresour Technol* 118:536–544. <https://doi.org/10.1016/j.biortech.2012.05.042>
 37. Ahmed MB, Zhou JL, Ngo HH, Guo W, Chen M (2016) Progress in the Preparation and Application of Modified Biochar for Improved Contaminant removal from Water and Wastewater. *Bioresour Technol* 214:836–851. <https://doi.org/10.1016/j.biortech.2016.05.057>
 38. Zouari M, Devallance DB, Marrot L (2022) Effect of biochar addition on mechanical properties, thermal stability, and water resistance of hemp-poly(lactic acid) (PLA) composites. *Materials* 15:2271. <https://doi.org/10.3390/ma15062271>
 39. Arrigo R, Bartoli M, Malucelli G (2020) Poly(Lactic Acid)-Biochar Biocomposites: Effect of Processing and Filler Content on Rheological, Thermal, and Mechanical Properties. *Polymers* 12:892. <https://doi.org/10.3390/POLYM12040892>
 40. Infurna G, Botta L, Maniscalco M, Morici E, Caputo G, Marullo S, D'Anna F, Dintcheva NT (2022) Biochar Particles Obtained from Agricultural Carob Waste as a Suitable Filler for Sustainable Biocomposite Formulations. *Polymers* 14:3075. <https://doi.org/10.3390/polym14153075>
 41. Tomczyk A, Sokołowska Z, Boguta P (2020) Biochar Physico-chemical properties: Pyrolysis Temperature and Feedstock Kind effects. *Rev Environ Sci Biotechnol* 19:191–215. <https://doi.org/10.1007/s11157-020-09523-3>
 42. Vardon DR, Moser BR, Zheng W, Witkin K, Evangelista RL, Strathmann TJ, Rajagopalan K, Sharma BK (2013) Complete Utilization of Spent Coffee Grounds to produce Biodiesel, Bio-oil, and Biochar. *ACS Sustain Chem Eng* 1:1286–1294. <https://doi.org/10.1021/sc400145w>
 43. Kane S, Ryan C (2022) Biochar from food waste as a sustainable replacement for carbon black in upcycled or compostable composites. *Compos Part C Open Access* 8:100274. <https://doi.org/10.1016/j.jcomc.2022.100274>
 44. Giorcelli M, Bartoli M (2019) Development of coffee biochar filler for the production of electrical conductive reinforced plastic. *Polymers* 11:1916. <https://doi.org/10.3390/polym11121916>

45. Mayakrishnan V, Mohamed JK, Selvaraj N, SenthilKumar D, Annadurai S (2023) Effect of Nano-Biochar on Mechanical, Barrier and Mulching properties of 3D printed thermoplastic polyurethane Film. *Polym Bull* 80:6725–6747. <https://doi.org/10.1007/s00289-022-04380-2>
46. Giorcelli M, Khan A, Pugno NM, Rosso C, Tagliaferro A (2019) Biochar as a cheap and environmental friendly filler able to Improve Polymer Mechanical properties. *Biomass Bioenergy* 120:219–223. <https://doi.org/10.1016/j.biombioe.2018.11.036>
47. Haeldermans T, Samyn P, Cardinaels R, Vandamme D, Vanreppelen K, Cuypers A, Schreurs S (2021) Bio-based poly(3-Hydroxybutyrate)/Thermoplastic starch composites as a host matrix for Biochar Fillers. *J Polym Environ* 29:2478–2491. <https://doi.org/10.1007/s10924-021-02049-x>
48. Haeldermans T, Samyn P, Cardinaels R, Vandamme D, Vanreppelen K, Cuypers A, Schreurs S (2021) Poly(lactic Acid) biocomposites containing Biochar particles: effects of Fillers and Plasticizer on Crystallization and Thermal properties. *Express Polym Lett* 15:343–360. <https://doi.org/10.3144/expresspolymlett.2021.30>
49. Botta L, Teresi R, Titone V, Salvaggio G, La Mantia FP, Lopresti F (2021) Use of biochar as filler for biocomposite blown films: structure-processing-properties relationships. *Polymers* 13:3953. <https://doi.org/10.3390/polym13223953>
50. Maniscalco M, Infurna G, Caputo G, Botta L, Dintcheva NT (2021) Slow pyrolysis as a method for biochar production from carob waste: process investigation and products' characterization. *Energies* 14:8457. <https://doi.org/10.3390/en14248457>
51. George J, Jung D, Bhattacharyya D (2023) Improvement of Electrical and Mechanical properties of PLA/PBAT composites using Coconut Shell Biochar for Antistatic Applications. *Appl Sci* 13:902. <https://doi.org/10.3390/app13020902>
52. Musioł M, Ryz J, Janeczek H, Kordyka A, Andrzejewski J, Sterzyński T, Jurczyk S, Cristea M, Musioł K, Kampik M et al (2022) (Bio)degradable biochar composites—Studies on degradation and electrostatic properties. *Mater Sci Eng* 275:115515. <https://doi.org/10.1016/j.mseb.2021.115515>
53. Abdel-Azim A-AA, Atta AM, Farahat MS, Boutros WY (1998) Determination of intrinsic viscosity of Polymeric compounds through a single specific viscosity measurement. *Polymer* 39:6827–6833. [https://doi.org/10.1016/S0032-3861\(98\)00184-0](https://doi.org/10.1016/S0032-3861(98)00184-0)
54. Meng Q, Heuzey M-C, Carreau PJ (2012) Control of Thermal degradation of Polylactide/Clay nanocomposites during Melt Processing by Chain Extension reaction. *Polym Degrad Stab* 97:2010–2020. <https://doi.org/10.1016/j.polymdegradstab.2012.01.030>
55. Andrade MF, Filho LEPT, de Silva M, de Lima ID, Carvalho JC, Almeida LH, Vinhas YMB (2020) Influence of gamma radiation on the properties of biodegradable PBAT – Poly (Butylene Adipate Co-terephthalate) active films with orange essential oil. *Macromol. Symp.* 394:2000057. <https://doi.org/10.1002/masy.202000057>
56. El-Sayed SA, Mostafa ME (2015) Kinetic parameters determination of Biomass Pyrolysis Fuels using TGA and DTA techniques. *Waste Biomass Valorization* 6:401–415. <https://doi.org/10.1007/s12649-015-9354-7>
57. Liu Y, He Z, Uchimiya M (2015) Comparison of Biochar formation from various Agricultural By-Products using FTIR Spectroscopy. *Mod Appl Sci* 9:p246. <https://doi.org/10.5539/mas.v9n4p246>
58. Lee Y, Park J, Ryu C, Gang KS, Yang W, Park Y-K, Jung J, Hyun S (2013) Comparison of Biochar Properties from Biomass residues produced by slow pyrolysis at 500°C. *Bioresour Technol* 148:196–201. <https://doi.org/10.1016/j.biortech.2013.08.135>
59. Socrates G (2001) Infrared and Raman characteristic group frequencies tables and charts, 3rd edn. Wiley, Newyork
60. Arrigo R, Dintcheva NT, Guenzi M, Gambarotti C, Filippone G, Coiai S, Carroccio S (2015) Thermo-oxidative resistant nanocomposites containing Novel hybrid-nanoparticles based on natural polyphenol and Carbon Nanotubes. *Polym Degrad Stab* 115:129–137. <https://doi.org/10.1016/j.polymdegradstab.2015.02.014>
61. La Mantia FP, Dintcheva NT, Malatesta V, Pagani F (2006) Improvement of Photo-Stability of LLDPE-Based nanocomposites. *Polym Degrad Stab* 91:3208–3213. <https://doi.org/10.1016/j.polymdegradstab.2006.07.014>
62. Botta L, Scaffaro R, La Mantia FP, Dintcheva NT (2010) Effect of different matrices and nanofillers on the Rheological Behavior of Polymer-Clay nanocomposites: Rheological Behavior of Polymer-Clay nanocomposites. *J Polym Sci Part B Polym Phys* 48:344–355. <https://doi.org/10.1002/polb.21896>
63. Codou A, Anstey A, Misra M, Mohanty AK (2018) Novel Compatibilized Nylon-based Ternary blends with polypropylene and poly(lactic acid): morphology evolution and Rheological Behaviour. *RSC Adv* 8:15709–15724. <https://doi.org/10.1039/C8RA01707G>
64. Lacroix C, Grmela M, Carreau PJ (1998) Relationships between Rheology and morphology for Immiscible Molten Blends of Polypropylene and Ethylene Copolymers under Shear Flow. *J Rheol* 42:41–62. <https://doi.org/10.1122/1.550943>
65. Li K, Peng J, Turng L-S, Huang H-X (2011) Dynamic rheological behavior and morphology of Polylactide/Poly(Butylenes Adipate-Co-Terephthalate) blends with various composition ratios. *Adv Polym Technol* 30:150–157. <https://doi.org/10.1002/adv.20212>
66. Scaffaro R, Sutera F, Mistretta MC, Botta L, La Mantia FP (2017) Structure-properties relationships in Melt Reprocessed PLA/Hydroxycalcites nanocomposites. *Express Polym Lett* 11:555–564. <https://doi.org/10.3144/expresspolymlett.2017.53>
67. Li X, Gong S, Yang L, Zhang F, Xie L, Luo Z, Xia X, Wang J (2020) Study on the degradation behavior and mechanism of poly(lactic acid) modification by Ferric Chloride. *Polymer* 188:121991. <https://doi.org/10.1016/j.polymer.2019.121991>

Authors and Affiliations

Giulia Infurna¹ · Luigi Botta¹ · Irene Ingargiola¹ · Marco Maniscalco¹ · Giuseppe Caputo¹ · Nadka Tz. Dintcheva¹

✉ Luigi Botta
luigi.botta@unipa.it

Giulia Infurna
giulia.infurna@unipa.it

Marco Maniscalco
marco.maniscalco02@unipa.it

Giuseppe Caputo
giuseppe.caputo01@unipa.it

Nadka Tz. Dintcheva
nadka.dintcheva@unipa.it

¹ Dipartimento di Ingegneria, Università degli Studi di Palermo, Viale delle Scienze, Ed. 6, 90128 Palermo, Italy